A New Approach to Accelerometer-based Head Tracking for Augmented Reality & Other Applications

M. S. Keir[1,2], C. E. Hann[1], J. G. Chase[1], and X. Q. Chen[1]
[1]Department of Mechanical Engineering,
[2]Human Interface Technology Lab NZ,
University of Canterbury
Private Bag 4800, Christchurch, New Zealand
matthew.keir@hitlabnz.org

***Abstract*— This work seeks to improve dynamic accuracy of viewpoint tracking for Augmented Reality. Using an inverted pendulum to model the head, dynamic orientation sensing in a vertical plane is achieved using only a dual axis accelerometer. A unique solution is presented as conventional approaches to solve the model equations fail to produce stable results due to ill conditioning. Accuracy is limited by the noise and model error. However, dynamic tracking with better than 1° accuracy is achieved analytically and experimentally.**

I. INTRODUCTION

Augmented Reality (AR) systems using head mounted displays (HMDs) require position and orientation (pose) information of the users viewpoint to overlay computer imagery correctly. Tracking accuracy and system latency are crucial to providing a compelling and useful AR application. Robust tracking systems are available for quasi-static applications. However, when applied in more dynamic applications they fail to produce the accuracy required.

Many different technologies have been applied to the head tracking problem, although no one technology tracks well for all applications [1]. As a result hybrid approaches have been taken ([2], [3], [4]) to improve accuracy and robustness by utilising two or more complementary technologies. Inertial tracking is often included in such approaches.

The inertial measurement units (IMUs) used for head tracking usually contain micro-electro-mechanical systems (MEMS). Specifically, rate gyroscopes (gyros) and accelerometers. High update rates and small size reduces system latency and allows unobtrusive packaging. However, measurements from these accelerometers and gyros require integration to obtain position and orientation. Numerical integration of noisy signals causes the results to drift. For the gyro this drift requires correction. However with the accelerometer drift corrupts the position measurement entirely due to the double integration. Hence, inertial devices are only useful for tracking orientation in this application. Importantly AR systems are more sensitive to orientation error than position error, as the orientation error is scaled by the distance to the viewed object [5].

Accelerometers sense dynamic accelerations and also the acceleration due to gravity. As a result accelerometers can be very useful in tilt or orientation applications. For a stationary object determining the orientation with respect to gravity is a trivial problem. However, when other motion is introduced the acceleration signal is modified by the dynamic accelerations, leading to orientation errors.

One approach to this problem is to take advantage of the burst like nature of head motion and correct for gyro drift during natural pauses [6]. However [7], shows orientation is improved using accelerometers to aid the gyroscope during human kinematic measurement, but does not detail the motion. Thus a full solution using only one sensor is lacking.

Commercial IMUs suitable for tracking 3DOF head motion include, the InertiaCube3 [8], 3d-Bird [9], MTx [10] and the 3DM-DH [11]. These IMUs typically contain three rate gyros, accelerometers and magnetometers. However, these devices are not optimised for individual applications although some allow the user to define initial filtering. None are yet fully proven in a highly dynamic environment.

Head motion for most applications is well below 2 Hz [12]. However, applications such as outdoor gaming demand much higher dynamic performance. Most approaches to improving dynamic tracking involve using Kalman filtering to fuse data from different sources and provide prediction to reduce system latency [13], [14]. The Kalman filter uses a model of the motion to predict for the next iteration step, this is not feasible with an unstable or unknown head motion model.

This paper seeks to improve inertial sensing for pitch and roll in a highly dynamic environment using minimal numbers of low cost sensors. Using an inverted pendulum to model the head, it is shown that dynamic orientation sensing can be achieved using only accelerometers. The results offer some potentially unique outcomes in application spaces such as robotics and manufacturing, and head motion sensing for AR.

II. METHOD

A. Model – Rotation in a Vertical Plane

An inverted pendulum model applies where a mass is balanced above an axis of rotation. This balanced equilibrium state is intrinsically unstable. In this application the head is supported by cervical spine above the shoulders and stability maintained by applied forces from the neck musculature. Gillies uses an inverted pendulum model to explore the dynamics of head motion [15]. The model is verified with

some experimental data though they fail to solve the model for rotational angle over any useful time period.

In this work the inverted pendulum is used to model the head with a dual axis accelerometer positioned along the pendulum, in the plane of rotation (2D). The radius of rotation for the head may be modelled as a function of the degree of rotation due to the flexibility of the cervical spine. However, for this proof of concept the radius is considered to be fixed.

Fig. 1 shows the components of acceleration applied to a particle at radius R for in-plane rotation ($\theta(t)$) of the head or pendulum. These tangential, centripetal and gravitational (g) accelerations and are sensed by the accelerometer axes $A_y(t)$ and $A_x(t)$. The accelerometer is positioned at a fixed angle λ to the tangent of rotation, where $\lambda = \pi/4$ provides optimal sensitivity to gravity on both accelerometer axes. It also ensures the other accelerations are sensed by both axes which is useful to abate noise.

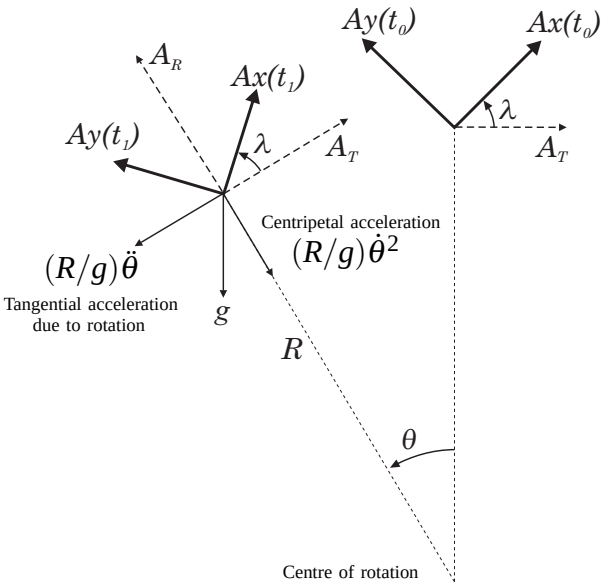

Fig. 1. Acceleration vector diagram for a point at the end of an inverted pendulum, length R, undergoing a rotation of θ

The tangential ($A_T(t)$) and radial ($A_R(t)$) accelerations are derived from the measured accelerations below. Note that all accelerations and rotations ($\theta(t)$) are functions of time and that the "(t)" is dropped for clarity.

$$A_T = A_x\cos(\lambda) - A_y\sin(\lambda), \tag{1}$$

$$A_R = A_x\sin(\lambda) + A_y\cos(\lambda). \tag{2}$$

The accelerometer senses the acceleration of its proof mass relative to its casing. Hence, dynamic accelerations contribute in the opposite direction to that shown in Fig. 1. Resolving acceleration components in terms of g along the tangential and radial axes provides two independent ordinary differential equations (ODEs) for A_T and A_R:

$$A_T = (R/g)\ddot{\theta} - \sin(\theta), \tag{3}$$

$$A_R = (R/g)\dot{\theta}^2 - \cos(\theta). \tag{4}$$

It is important to note that these are not equations of motion, and are thus is independent from any inertia, actuation force, damping or physiological limits that may influence the motion. The effect of any such terms will directly contribute the measured acceleration and is therefore captured by this model. This approach frees the problem from complex calibration or system identification procedures.

B. A General Engineering Approach

Solving Equations (3) or (4), should provide the solution for θ. As a first attempt, data is generated for θ from a modified sine wave. The tangential acceleration is determined by substituting θ into Equation (3). This ODE was solved in Maple using the default initial value problem (IVP) solver, a Fehlberg fourth-fifth order Runge-Kutta method, and in Matlab using a similar solver. Both Maple and Matlab failed to produce a stable solution.

Providing the solver with the actual initial conditions, $\theta(0)$ and $\dot{\theta}(0)$, results in the solution tracking the true solution for only two cycles before diverging. This result represents the pendulum spinning in the real system. Fig. 2 shows that with a very low amplitude for θ the solution almost stabilises at π. Similar quasi-stability can be found at $-\pi$ when the pendulum is no longer inverted, a stable solution for the real pendulum. Including a damping term in the ODE can stabilise this solution. However, it proves to be of no use in determining the true rotation.

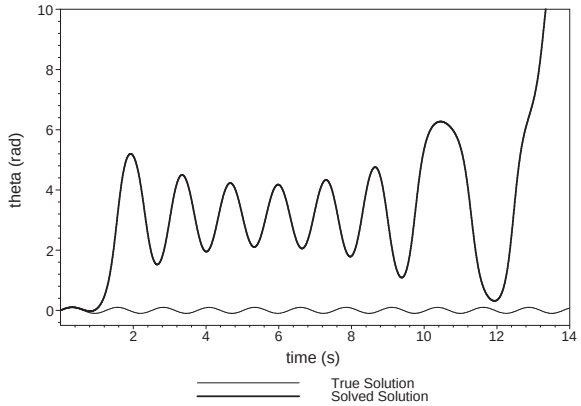

Fig. 2. Simulated data, solved numerically. Note the that the solved solution oscillates around Pi before blowing up completely

A second attempt combines the Equations, (3) and (4). Solving simultaneously also fails to produce a stable result. To gain a better understanding of the instability of the model and enable an analytical solution Equation (3) is linearised:

$$A_T = (R/g)\ddot{\theta} - \theta \tag{5}$$

Giving an analytic solution of the form:

$$\theta = C_2 e^{\frac{\sqrt{g}}{\sqrt{R}}t} + C_1 e^{-\frac{\sqrt{g}}{\sqrt{R}}t} - A_T \tag{6}$$

where C_1 and C_2 are constants. The positive power on the C_2 exponential term leads to instability. The system is extremely sensitive the the value of the C_2 and thus the initial conditions.

To illustrate this issue consider synthetic data generated from Equation (5). Solving using the exact initial conditions provides the true solution. However, introducing a small error to the $\dot{\theta}$ initial condition ε makes the solution unstable. Fig. 3 illustrates this ill conditioning when the error is $\varepsilon = 1e^{-18}$. Even recursive approaches over a much shorter period will not work because any error will quickly grow and corrupt the solution.

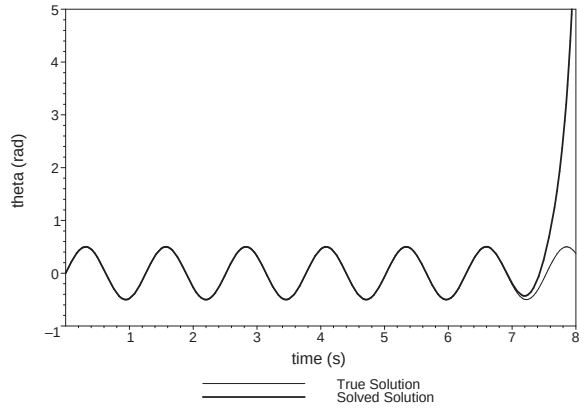

Fig. 3. Simulated linearised data, solved analytically using initial conditions with a small error

C. Feasible Solution Method

It is clear that this challenging problem requires a novel approach. This section presents a unique solution independent from initial conditions to obtain C_2 with the precision required to give accurate rotational measurement.

Linearising Equation (3) in terms of θ over a short time interval provides an equation that can be solved analytically. This linearisation requires a substitution for $\sin(\theta)$:

$$sin\_theta(\theta) = b_1 + b_2\theta \tag{7}$$

where b_1 and b_2 are evaluated by a linear least squares fit to $\sin(\theta_{old})$ over the last 0.1 seconds. θ_{old}, a vector of the past orientation values, is initially unknown. In this instance a vector containing zeros is used. A cubic fit over the same period for A_T effectively filters higher frequency noise:

$$A_{T,fit} = a_1 + a_2 t + a_3 t^2 + a_4 t^3 \tag{8}$$

However, these polynomial fits assume that 0.1 seconds is much less than the period of the motion. Increasing frequency of the motion will ultimately result in a reduction in the quality of the fit and algorithm solution.

Substituting Equation (7) and (8) into Equation (3) gives:

$$A_{T,fit} = (R/g)\ddot{\theta} - sin\_theta(\theta) \tag{9}$$

Solving Equation (9) gives θ_{sol}, the numerical solution for the linearised tangential ODE, defined:

$$\theta_{sol} = C_2 e^{(mt)} + C_1 e^{(-mt)} + f(t) \tag{10}$$

where C_1 and C_2 are unknown constants and:

$$m = \frac{\sqrt{(b_2 g)}}{\sqrt{R}}$$

$$f(t) = \frac{1}{{b_2}^2 g}\Big(-gb_2(b_1 + a_1 + a_2 t + a_3 t^2 + a_4 t^3) - 2R(3a_4 t + a_3)\Big)$$

Equation (10) is very sensitive to the solution for C_2, as illustrated earlier. The approach taken here is to utilise the independent radial Equation, (4) to solve for C_1 and C_2. The $\cos(\theta)$ term is approximated by a least squares fit to a quadratic function over the last 0.1 seconds:

$$cos\_theta(\theta) = c_1 + c_2\theta + c_3\theta^2 \tag{11}$$

This removes the nonlinear cosine function without increasing the order of the ODE. Substituting Equations (10) and (11) into Equation (4):

$$A_{R,sol} = (R/g)\dot{\theta}_{sol}^2 - cos\_theta(\theta_{sol}) \tag{12}$$

To find the optimal C_1 and C_2 values a least squares approach fits $A_{R,sol}$ to the measured radial acceleration, Equation (2), over the last 0.1. Two independent equations are required which are obtained by differentiating with respect to each constant.

$$Eq_A = \frac{d}{dC_1}\left(\sum_{i=1}^{10}\Big(A_{R,sol}(t-i) - A_R(t-i)\Big)^2\right) \tag{13}$$

$$Eq_B = \frac{d}{dC_2}\left(\sum_{i=1}^{10}\Big(A_{R,sol}(t-i) - A_R(t-i)\Big)^2\right) \tag{14}$$

Simultaneously solving Equations (13) and (14), provides nine pairs of solutions. The real pair that minimises the following equation are selected.

$$Eq_C = \left(\sum_{i=1}^{10}\Big(A_{R,sol}(t-i) - A_R(t-i)\Big)^2\right)^{1/2} \tag{15}$$

The selected C_1 and C_2 are substituted into Equation (10) to give orientation for the current time step. θ_{old} can then be updated ensuring an accurate fit is achieved for the trigonometric terms in Equations (7) and (11) for the next time step. Fig. 4 summarises this method in a flow-chart.

D. Analysis and Performance Metrics

The method is validated using both experimental and synthetic data. Due to the symmetric nature of head motion [16], it is reasonable to use a modified sine wave as basic representative head motion. Allowing the algorithm to be easily tested with different dynamics and noise. The main goals include:

- Verify the model using experimental data from an inverted pendulum.
- An analysis to determine the robustness to noise using synthetic data.
- Determine the dynamic performance of the method.
- Test the method with experimental data.

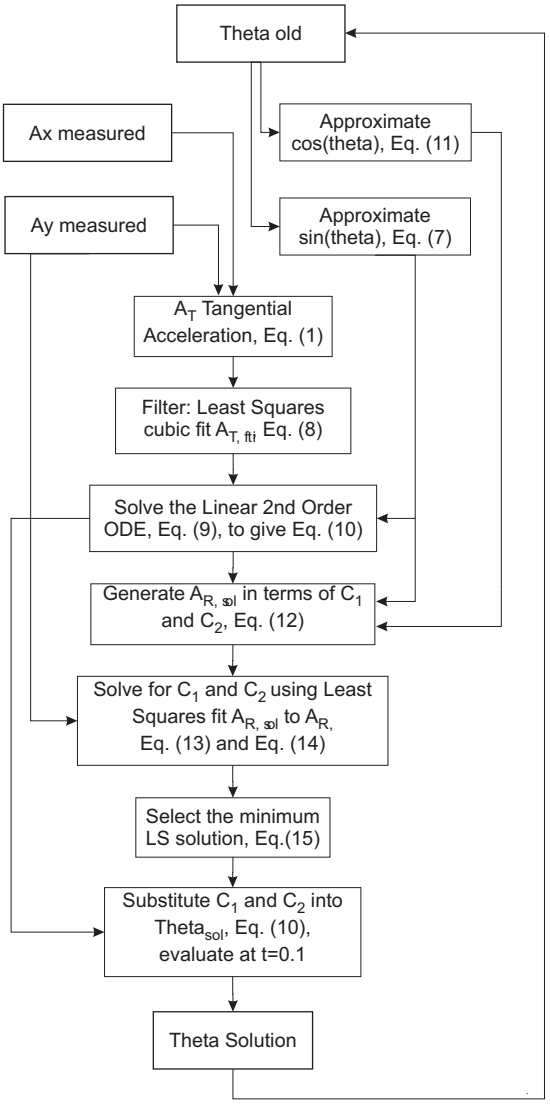

Fig. 4. Flow-chart for the solution of θ

To measure and quantify performance, the mean absolute error is calculated. For the synthetic data, error is defined as the difference between the solution and the θ used to generate the acceleration signals. For the experimental data the error is the difference between the solution and the optical encoder measurement. Standard deviation will measure the spread of the fit. These performance metrics are calculated after any initial transient behaviour in the solution has died away.

III. RESULTS AND DISCUSSION

A. Model Verification

To verify that Equations (3) and (4) fit the model of the inverted pendulum a simple experiment was conducted. An existing inverted pendulum apparatus was used with an optical encoder providing an independent measure of rotation, θ_{en}. The encoder used had a resolution and nominal position error of 0.17°. An Analogue Devices ADXL213 dual axis accelerometer was attached to the pendulum at radius $R = 0.3$m, and at an angle $\lambda = \pi/4$. Data was collected while manually moving the pendulum.

Estimates of the true A_x and A_y were generated by first calculating A_T and A_R using θ_{en} and the model Equations (3) and (4). To combat the buildup of noise due to the differentiation of θ_{en}, this signal is filtered to smooth the steps caused by the finite resolution of the encoder. The tangential and radial accelerations derived were then resolved along the accelerometer axes giving x and y axis accelerations for the model, $A_{x,\,mod}$ and $A_{y,\,mod}$.

$$A_{x,\,mod} = A_T\cos(\lambda) + A_R\sin(\lambda) \quad (16)$$

$$A_{y,\,mod} = A_R\cos(\lambda) - A_T\sin(\lambda) \quad (17)$$

A comparison of the measured A_x and $A_{x,\,mod}$ is shown in Fig. 5. Similar results can be shown for A_y accelerometer axis. Table I summarises the acceleration error. This error is within approximately 1.4% of the amplitude in Fig. 5.

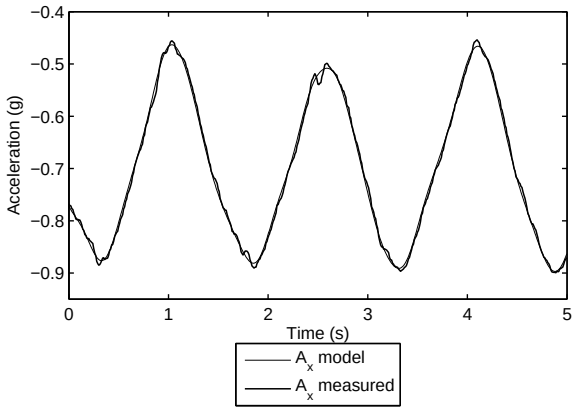

Fig. 5. Experimental comparison of the measured x-axis acceleration and that generated using the model equations

TABLE I
MODEL ERROR IN TERMS OF ACCELERATION

Acceleration Error	A_x (mg)	A_y (mg)
Mean	6.3	6.2
Standard Deviation	4.0	3.8

To determine the accuracy of the model fit to the experimental data in terms of θ, independently from the solution method and noise, Equation (3) is integrated giving:

$$\frac{R}{g}(\theta - \dot{\theta}(0)t - \theta(0)) = \int_0^t\int_0^t A_T + \int_0^t\int_0^t \sin(\theta), \quad (18)$$

Fitting Equation (18) to the experimental data determines the optimal initial conditions for the chosen period. This fit could also be used to find an optimal R value for later calibration procedures, but here the measured R is used. Equation (18) is rearranged to give θ:

$$\theta = \frac{g}{R}\int_0^t\int_0^t A_T + \frac{g}{R}\int_0^t\int_0^t \sin(\theta) + \dot{\theta}(0)t + \theta(0), \quad (19)$$

Evaluating the right hand side for the experimental data and comparing the result to θ_{en}, as shown in Fig. 6, determines the model error. These results are shown in Table II and illustrate that error is present. However, the mean error is less than 1° in a highly dynamic situation. This result verifies that the inverted pendulum model does capture the main dynamics for this situation. Explanations for the remaining model error include:

- Missing dynamics due to finite encoder precision.
- Errors in the initial set up, placement of the accelerometer, and zero position of the pendulum.
- Out of plane disturbances affecting the accelerometers.

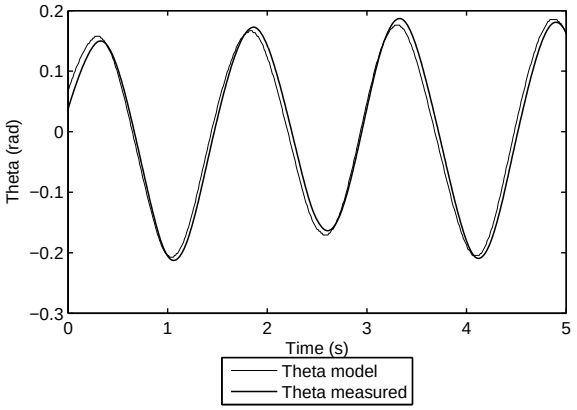

Fig. 6. Comparison of the measured theta and theta derived from the tangential model equation

TABLE II
MODEL ERROR IN TERMS OF THETA

Theta Error	Tangential Equation
Mean (deg)	0.81
Standard Deviation (deg)	0.46

B. Robustness to Noise

Noise on the acceleration signals which drive the solutions to the ODE are comprised of two sources. First, the high frequency raw noise from the accelerometer and circuitry. Second, a lower frequency model error that may include motion not captured by the encoder. The method is tested using synthetic data at three noise levels from no noise up to the maximum expected nose based on experiments. These results are shown in Table III and are within 1° error. However, there are some larger standard deviations due to the switching between solutions of the algorithm in Equation (15).

Calculating rotation using a quasi-static or simple approach assumes that the change in tangential acceleration is due only to rotation. Thus, taking the inverse sine of A_T yields the simple solution shown in Fig. 7 for comparison. Note that the solved solution starts at zero. This is the initial estimate for the θ_{old} vector and illustrates the independence from initial conditions with the solved solution quickly converging to the true solution.

TABLE III
ERROR RESPONSE TO THE PRESENCE OF NOISE

Mean Absolute Noise	Mean Error (deg)	Standard Deviation (deg)
None (0mg)	0.0001	0.0002
Medium (3.3mg)	0.34	0.31
Medium Shifted	*0.27*	*0.16*
Maximum (8.3mg)	0.52	0.45

Further investigation shows that the noise present is not of constant magnitude with respect to θ. Recall that the accelerometer is positioned at $\lambda = \pi/4$ to provide optimal resolution on both axes. However, the radial acceleration generated using Equation (2) will still suffer from poor resolution.

To improve this situation the medium noise case was repeated with the pendulum rotated by adding 45 degrees, and $\lambda = 0$ thus, aligning the accelerometer axes with the radial and tangential axes. Solving for rotation yields a mean error of 0.27°, an improvement of 0.07° over the initial accelerometer placement. These results are compared in Fig. 7. However, this improvement can not be solely attributed to improving the resolution of the radial ODE as this is only used to select the best solution. Shifting the accelerometer placement also separates the nine solutions to the tangential ODE, allowing easier selection of the correct solution.

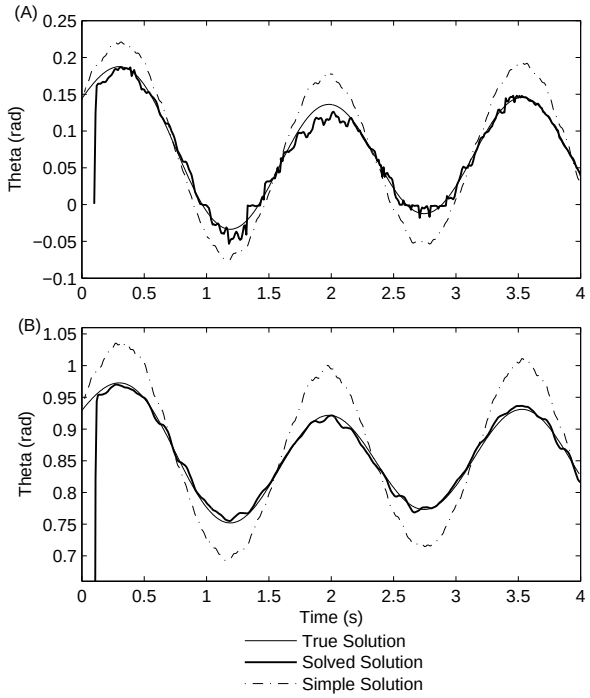

Fig. 7. Method results for simulated data with moderate noise applied (A), and improved result when shifted by 45° (B)

C. Dynamic Performance

One of the key drivers for this work is to improve on orientation accuracy in a fully dynamic application. To quantify the dynamic performance of the algorithm presented, synthetic data of different frequency and amplitude tested. Fig. 8 illustrates how the error in the solution responds with increasing dynamics. Tests are run with the same noise for two different amplitudes, small rotations of 3°, and medium rotations of 10°. The quasi-static or simple solution is included for comparison.

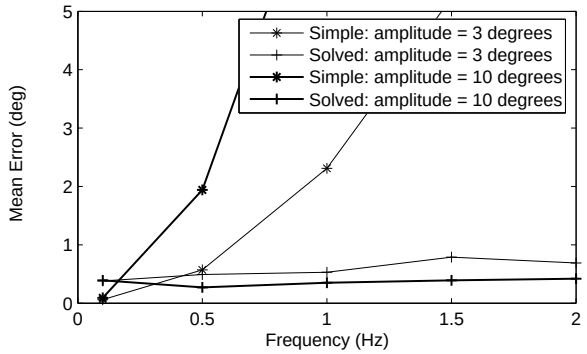

Fig. 8. The response of the algorithm to increasing dynamics

The algorithm presented shows stable performance with increasing dynamics. However, the accuracy is ultimately limited by the noise on the acceleration signals. The results for the quasi-static method clearly show that it's use is rightly limited to stationary or near stationary orientation measurements, but does provide results better than the algorithm developed in these situations.

D. Experimental Results

An experiment was run on the inverted pendulum apparatus as before, and the algorithm used to solve for rotation. A comparison of the solution to the reference encoder signal is shown in Fig. 9 and error metrics in Table IV.

TABLE IV
ERROR RESULTS FOR EXPERIMENTAL DATA

Theta Error	Real Data
Mean (deg)	0.39
Standard Deviation (deg)	0.33

IV. CONCLUSIONS

Viewpoint tracking methods for augmented reality applications that use HMDs generally suffer from poor dynamic performance. This work achieves dynamic orientation tracking for a single degree of rotation in the vertical plane using only a dual axis accelerometer. Head motion is modelled by that of an inverted pendulum, however instability in the model results in ill conditioning and can not be solved using conventional methods. A unique approach that is independent of initial conditions is presented and evaluated with synthetic and experimental data.

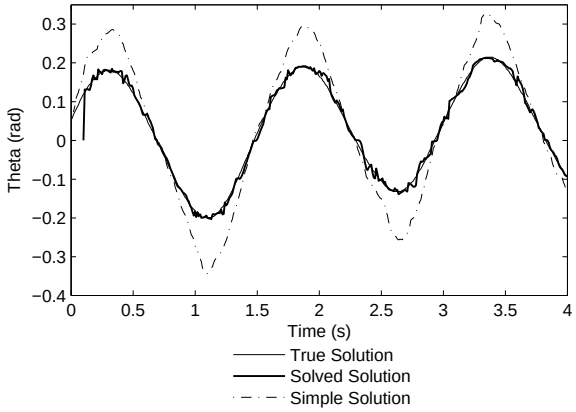

Fig. 9. Experimental results comparing the solved solution to the encoder

The algorithm presented produces good results with mean error better than 1° for synthetic and experimental data. The integrity of this result is maintained as the dynamics are increased and it does not suffer from drift. The accuracy of the solution is limited by the model error and noise. Latency introduced by this solving method has not been considered. This work proves the initial concept of using an accelerometer to measure dynamic head rotation in a vertical plane.

REFERENCES

[1] G. Welch and E. Foxlin, "Motion tracking: No silver bullet, but a respectable arsenal," *IEEE Computer Graphics and Applications*, vol. 22, no. 6, pp. 24–38, 2002.

[2] G. W. Roberts, A. Evans, A. Dodson, B. Denby, S. Cooper, and R. Hollands, "The use of augmented reality, gps, and ins for subsurface data visualization." in *FIG XXII International Congress*, Washington, D.C, April 2002.

[3] S. You, U. Neumann, and R. Azuma, "Orientation tracking for outdoor augmented reality registration," *IEEE Computer Graphics and Applications*, vol. 19, no. 6, pp. 36–42, Nov./Dec. 1999.

[4] E. Foxlin and L. Naimark, "VIS-tracker: A wearable vision-inertial self-tracker," in *VR*. IEEE Computer Society, 2003, pp. 199–206.

[5] R. L. Holloway, "Registration error analysis for augmented reality," *Presence: Teleoperators and Virtual Environments*, vol. 6, no. 4, pp. 413–432, 1997.

[6] E. Foxlin, M. Harrington, and Y. Altshuler, "Miniature 6-DOF inertial system for tracking HMDs," in *Proceedings of the SPIE*, vol. 3362, Orlando, FL, 1998, pp. 214–228.

[7] H. Luinge, P. Veltink, and C. Baten, "Estimation of orientation with gyroscopes and accelerometers," in *BMES/EMBS Conference, 1999. Proceedings of the First Joint*, vol. 2, 1999, p. 844.

[8] "http://www.isense.com/."

[9] "http://www.ascension-tech.com/."

[10] "http://www.xsens.com/."

[11] "http://www.microstrain.com/."

[12] R. Azuma and G. Bishop, "A frequency-domain analysis of head-motion prediction," in *SIGGRAPH*, 1995, pp. 401–408.

[13] E. Kraft, "A quaternion-based unscented kalman filter for orientation tracking," in *Proceedings of the 6th Int. Conf. on Information Fusion*, Cairns, Australia, July 2003.

[14] L. Chai, K. Nguyen, B. Hoff, and T. Vincent, "An adaptive estimator for registration in augmented reality," in *Proceedings of IEEE International Workshop on Augmented Reality*, 1999, pp. 23–32.

[15] G. T. Gillies, D. W. Christy, J. M. Stenger, and W. C. Broaddus, "Equilibrium and non-equilibrium dynamics of the cranio-mandibular complex and cervical spine," *Journal of Medical Engineering & Technology*, vol. 27, no. 1, pp. 32–40, January 2003.

[16] C. Shaw and J. Liang, "An experiment to characterize head motion in VR and RR using MR," in *Proceedings of the 1992 Western Computer Graphics Symposium*, 1992, pp. 99–101.